



## Effect of Process Parameters on the Metallurgical Properties of a Boron-Added Cast Austenitic Steel Designed for Special Purposes

### Özel Amaçlara Yönelik Tasarlanmış Bor Katkılı bir Dökme Ostenitli Çeliğin Metalurjik Özelliklerine İşlem Parametrelerinin Etkisi

Ersel Aydın<sup>1</sup> , Fikri Erdem Şeşen<sup>2\*</sup> , Selim Coşkun<sup>3</sup> , Cevat Fahir Arısoy<sup>3</sup> 

<sup>1</sup>Önerler Heat Treatment Co., BTSO Industrial Zone, Turuncu Str 12, 1610, Nilüfer-Bursa, TÜRKİYE

<sup>2</sup>Kırıkkale University, Metallurgical and Materials Engineering Department, 71450 Kırıkkale, TÜRKİYE

<sup>3</sup>Istanbul Technical University, Metallurgical and Materials Engineering Department, 34469 İstanbul, TÜRKİYE

Başvuru/Received: 12/09/2023

Kabul / Accepted: 22/11/2023

Çevrimiçi Basım / Published Online: 31/01/2024

Son Versiyon/Final Version: 31/01/2024

#### Abstract

A new kind of boron-added cast austenitic steel which also contained significant amounts of chromium, molybdenum and manganese was manufactured via vacuum induction melting followed by casting procedure. Solution annealing heat treatment was performed at three different temperatures for three different times to dissolve eutectic  $M_2C$  carbides in austenitic matrix. All samples were rapid-cooled in an oil medium after the solution annealing heat treatment. Aging treatments were carried out after solution annealing heat treatment performed at 1250 °C for 24 hours. Hardness value was decreased after solution annealing performed at 1250 °C for 24 hours. Transformation of  $M_2C$  carbide with a hexagonal lattice into Fe-rich  $M_6C$  carbide with a face-centered cubic lattice and formation of precipitates occurred as a result of aging performed at 700 and 800 °C. Submicron-sized  $Cr_{23}C_6$  carbides and  $Mo_2BC$  precipitates were formed and hardness value was increased after aging performed at 700 °C. Nano-sized  $Cr_{23}C_6$  carbides,  $Mo_2B$  borides and  $Cr_7BC_4$  precipitates were formed and hardness value was higher after aging performed at 800 °C. An optical light microscope was utilized to characterize solution annealing treatments and to perform grain size measurements. A scanning electron microscope was used to identify carbide types and carbide transformation during aging. Carbide and boride precipitates were detected by using a transition electron microscope.

#### Key Words

“Vacuum induction melting, Cast austenitic steel, Heat treatment, Precipitation hardening, Carbide and boride precipitate, Carbide transformation”

#### Öz

Yeni bir tür bor katkılı, aynı zamanda krom, molibden ve manganez içeren, dökme ostenitli çelik vakum indüksiyon ergitmenin ardından döküm yoluyla üretilmiştir. Ötektik  $M_2C$  karbürlerini ostenitli matriks içerisinde çözündürmek amacıyla üç farklı sıcaklıkta üç farklı süreyle çözeltiye alma ısıl işlemi uygulanmıştır. Çözeltiye alma ısıl işleminin ardından numunelerin tümü yağ ortamında hızlı soğutulmuştur. 1250 °C sıcaklıkta 24 saat süreyle uygulanmış çözeltiye alma ısıl işleminin ardından yaşlandırma işlemleri yapılmıştır. 1250 °C sıcaklıkta 24 saat süreyle uygulanmış çözeltiye alma işlemi sonucu sertlik değeri düşmüştür. 700 ve 800 °C sıcaklıklarda uygulanan yaşlandırma işlemleri sonucu hegzagonal kafes yapısındaki  $M_2C$  karbürünün yüzey merkezli kübik kafes yapısındaki demirce zengin  $M_6C$  karbürüne dönüşümü ve çökelti oluşumu meydana gelmiştir. 700 °C sıcaklıkta yapılan yaşlandırma işlemi sonucunda mikron altı boyutta  $Cr_{23}C_6$  karbürleri ve  $Mo_2BC$  çökeltileri oluşmuş ve sertlik değeri yükselmiştir. 800 °C sıcaklıkta yapılan yaşlandırma işlemi sonucunda da nano boyutta  $Cr_{23}C_6$  karbürleri,  $Mo_2B$  borürleri ve  $Cr_7BC_4$  çökeltileri oluşmuş ve sertlik değeri daha fazla yükselmiştir. Çözeltiye alma işlemlerinin karakterize edilmesi ve tane sınırı ölçümlerinin yapılması amacıyla bir ışık mikroskobu kullanılmıştır. Karbür tiplerinin ve yaşlandırma sırasında meydana gelen karbür dönüşümünün tanımlanması amacıyla bir taramalı elektron mikroskobu çalıştırılmıştır. Karbür ve borür çökeltilerinin varlığı aynı zamanda bir geçirimli elektron mikroskobu kullanılarak tespit edilmiştir.

#### Anahtar Kelimeler

“Vakum indüksiyon ergitme, Dökme ostenitli çelik, Isıl işlem, Çökelme sertleşmesi, Karbür ve borür çökeltmesi, Karbür dönüşümü”

## 1. Introduction

Austenitic steels are used in a wide range of areas. Their most used form is austenitic stainless steel, a type of stainless steel. Carbon is an undesired element in the chemical composition of all stainless steels and carbon content is very low in this kind of steels. On the other hand, specially alloyed austenitic steels which also include carbon are produced and used for special purposes, i.e. making hard and non-magnetic tools and equipment which have a high resistance to wear and are generally components of aerospace and automotive industries.

The phase of iron having a face-centered cubic crystal structure is called Austenite. The austenite phase, which does not exhibit magnetic behavior, is not thermodynamically stable at room temperature in unalloyed steels. Totten (2007) informed that merely steels that have convenient chemical compositions including certain alloying elements have an austenitic microstructure at room temperature.

Nickel, manganese, molybdenum, carbon and nitrogen are elements that make the austenitic microstructure thermodynamically stable in steels. According to Putatunda (2005), applying Equation 1 to a known chemical composition is considered a practical way to estimate over which temperature the austenite phase is thermodynamically stable in the related steel.

$$M_s = 561 - 475 \times C\% - 33 \times Mn\% - 17 \times Ni\% - 17 \times Cr\% - 21 \times Mo\% \quad [\text{Eq. 1}]$$

The alloying elements written down in Equation 1 decrease the lowest temperature at which the austenite phase is stable, depending on a certain coefficient, provided that they are in solution.

Excluding stainless steels, carbon content may be high in austenitic steels that are used for special purposes mentioned above. Some of the alloying elements in the chemical composition of these steels generate carbides with carbon. The tendency for carbide-forming behavior increases in the manganese, chromium and molybdenum sequence. The network-like appearance of these stable carbides leads to a brittle structure in the as-cast condition of this kind of steels produced by casting. Therefore, proper heat treatment procedures such as solution annealing followed by aging must be applied in order to homogenize the microstructure and optimize the properties.

Bhadeshia and Honeycombe (2006) stated that precipitation hardening can be applied in steels containing molybdenum, tungsten or vanadium, as well as steels with a high chromium content. Nevertheless, during the tempering of all alloy steels, alloy carbides are not formed until the temperature reaches 500–600 °C, because below this temperature range the metallic alloying elements cannot diffuse rapidly enough to permit alloy carbides to nucleate.

Düzçükoğlu and Çetintürk (2015) reported that a low amount of some elements like boron can be effective in steels and boron content of more than only 8 ppm is considered an alloy in steel according to a related standard (BS EN 10020:2000) that outlines the element content boundary between non-alloy and alloy steels. Boron atoms can be located in  $\alpha$ -iron, ferrite, in interstitial and substitutional positions. The reason for this is, stated by Sharma et al. (2019), that the atomic size ratio of boron to iron is 0.75, which is higher than 0.60 but lower than 0.85, the limits for location in the interstitial and the substitutional positions respectively. According to Çarboğa (2010), the maximum solubility of boron in  $\alpha$ -iron is 80 ppm at 910 °C while in  $\gamma$ -iron, austenite, it is 260 ppm at 1150-1170 °C. Boron is the most important alloying element to improve the hardenability of steel. Han et al. (2008) claimed that elemental boron, having been segregated along grain boundaries, prevents the nucleation of ferrite and pearlite by decreasing the interfacial energy of these regions. When elemental boron is excessively used, however, as stated by Suskia and Oliveira (2013), the hardenability of the steel is decreased since some preferential sites convenient for the generation of ferrite and bainite phases are provided because of  $Fe_{23}(B, C)_6$  structure which is precipitated along grain boundaries. Furthermore, in a review written by Sharma et al. (2019), it is outlined that boron content that is higher than 0.003 wt. % may cause a decrease in ductility and impact resistance, hot shortness, and an increase in sensitivity to overheating, thus these may lead to surface cracks during continuous casting and/or distortion during heat treatment.

The current work aimed to investigate the effects of the submicron and nano-sized phases formed due to precipitation hardening heat treatment in the microstructure of a boron-added austenitic cast steel on hardness. For revealing the effects of boron addition, a special high-carbon austenitic steel having significant amounts of manganese, chromium and molybdenum was generated and cast via the vacuum induction melting method. The influence of the microstructure that resulted from the applied solution annealing and aging treatments on hardness was observed for this purpose. Network-type eutectic  $M_2C$  carbides, which make the steel brittle and are formed during the solidification of cast austenitic steel, were dissolved in an austenitic matrix and then retained  $M_2C$ -type carbides evolved to spherical morphology by solution annealing treatment. Different solution annealing and aging temperatures were applied to obtain efficient precipitation hardening for different soaking times. Carbide precipitates such as  $Cr_3C_6$ ,  $Cr_7C_3$ ,  $Cr_{23}C_6$ ,  $Mo_2BC$ ,  $Cr_7BC_4$  and  $Mn_{23}C_6$  were generated as well as a boride precipitate,  $Mo_2B$ , as a result of different aging treatments. The microstructures that resulted from the solution annealing treatments were characterized by an optical light microscope.

Austenite grain size was measured using an image analyzing software incorporated into this optical light microscope. Hardness measurements were performed to observe the hardness change that resulted from the heat treatment processes. A Scanning Electron Microscope was used to identify the carbide types and carbide transformation during aging. Finally, a Transmission Electron Microscope was utilized in order to characterize the precipitates and detect the boron-related phases.

## 2. Experimental Procedure

The special cast austenitic steel which contained significant amounts of alloying elements such as manganese, chromium and molybdenum as well as a small amount of boron was manufactured via vacuum induction melting followed by casting procedure using ceramic shell molds in 45 mm diameter and 300 mm length. Chemical composition of the as-cast austenitic steel, which was detected by using an Optical Emission Spectrometer, is given in Table 1 together with standard deviation values. The convenient calibration procedure was applied to the spectrometer before the measurement.

**Table 1.** The Chemical Composition of The As-Cast Austenitic Steel In Wt. % With Standard Deviation Values

C	Si	Mn	P	S	Cr	Mo	B	Fe
0.75	0.35	4.00	0.025	0.035	5.96	4.71	0.0093	Balance
±0.029	±0.007	±0.1411	±0.005	±0.016	±0.42	±0.31	±0.00017	

Heat treatment processes were carried out in an electrical tube furnace under an argon atmosphere to prevent oxidation and decarburization. The samples which were used for solution annealing heat treatment were 45 mm in diameter and 25 mm in height. Different solution annealing treatments such as 1150 °C for 24 hours, 1200 °C for 24 hours and 1250 °C for 24, 48 and 72 hours were applied to dissolve carbides that were formed during the solidification of steel. All of the samples were rapid-cooled in an oil medium after solution annealing to maintain the super-saturated austenite phase and prevent any precipitation along grain boundaries during cooling.

Samples that were solution annealed at 1250 °C for 24 hours were cut into four equivalent pieces for aging treatment. Aging temperatures of 550, 600, 700 or 800 °C were applied to obtain efficient precipitation hardening and 1, 2, 3, 6, 9, 12 and 24 hours were chosen as soaking times for each aging treatment to investigate hardness changes precisely and determine the optimum aging duration. The related regions in binary phase equilibrium diagrams of Fe-C and Fe-B were considered for determining the selected temperatures and durations (Okamoto, H., 2004). Sharma et al. (2019) claim that the maximum solubility of boron in iron occurs at 1170 °C according to two Fe-B phase diagrams generated using Thermo-calc. Temperatures at which the solution annealing treatments were applied were selected close to this value. All heat treatment processes are schematically outlined in Figure 1.

Samples were prepared by grinding using SiC abrasive paper followed by polishing with alumina solution on a cloth and finally by electrolytic etching using an oxalic acid solution having a 5 wt. % purity during the application of electrical energy with a current density ranging between 0.1 and 0.2 A/cm<sup>2</sup>. Microstructural investigation of the cast austenitic steel was performed by using an optical light microscope, Olympus GX71. The austenite grain size was measured by the intercept method according to ASTM E112-13 (2021) standard using this optical light microscope incorporated with an image analyzing software.

Network-type eutectic and spherical carbides were examined under a Field Emission Scanning Electron Microscope (Jeol JSM 7000F) at an accelerating voltage of 15 kV. Backscattered Electron Imaging Compositional Mode was selected to highlight the microstructure. The chemical compositions of the carbides were analyzed by an energy-dispersive X-ray spectroscope (EDS) which was integrated into this Scanning Electron Microscope.

Hardness values were determined as the average of at least five measurements evaluated for each sample following the procedure for the Vickers indentation hardness test based on ASTM E92 (2023). Some hardness values measured incorrectly due to porosity in the samples were ignored. The standard deviation values for each heat treatment condition were evaluated using the STDEV function set up in Microsoft Excel.

A separate sample was solution annealed at 1235 °C for 10 hours followed by aging at 800 °C for 6 hours. Transmission Electron Microscopy (TEM) was utilized to identify and characterize the submicron-sized precipitates and for the detection of the boride phases formed within this sample. For this purpose, a Jeol 2000EX Transmission Electron Microscope was used at an acceleration voltage of 100 kV. Selected Area Electron Diffraction Patterns (SADP), Bright Field (BF) images and Dark Field (DF) images of the phases generated within the sample were obtained.

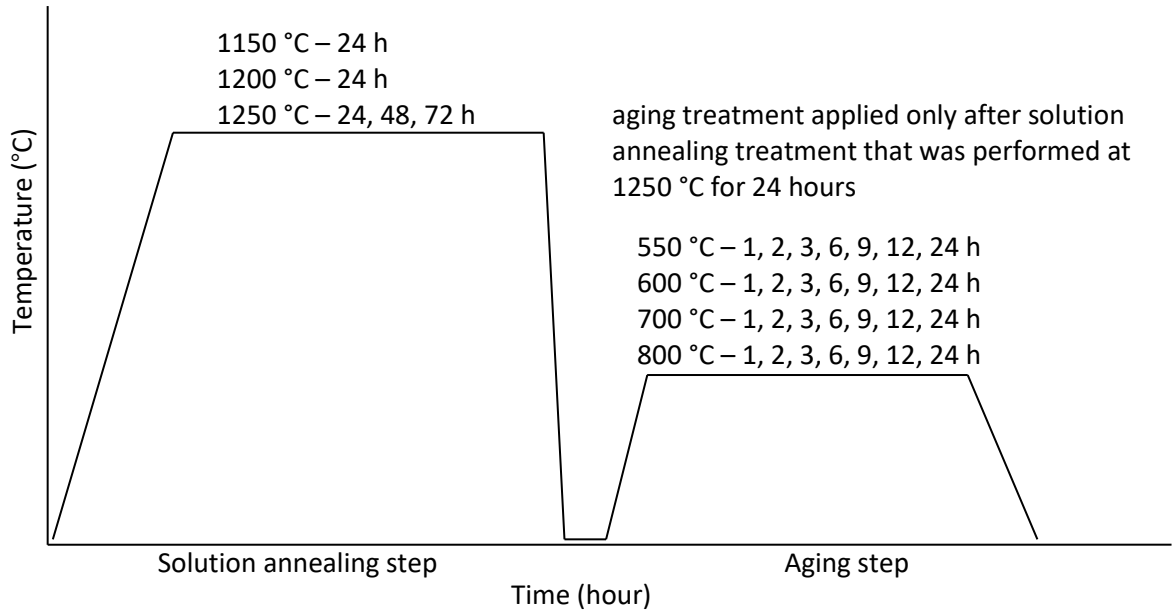


**Figure 1.** A Representative Scheme That Outlines the Heat Treatment Procedure Composed of Solution Annealing and Aging Steps

### 3. Results

Results of the microstructural observation and hardness measurement are given in this section.

#### 3.1 Microstructural Observation

##### 3.1.1 Optical light microscopy examination and grain size measurement

General microstructure of the as-cast austenitic steel is shown in the micrographs given in Figures 2-a and 2-b. Network-type eutectic  $M_2C$  carbides that extend along grain boundaries are easily seen in these micrographs. A microstructural image of the steel solution annealed at 1150 °C for 24 hours is given in Figure 3-a and that solution annealed at 1200 °C for 24 hours is given in Figure 3-b. It is understood that solution annealing treatments performed at 1150 and 1200 °C for 24 hours were not sufficient to dissolve the network-type eutectic  $M_2C$  carbides considering the similarity between these micrographs and the micrographs of the as-cast steel sample.

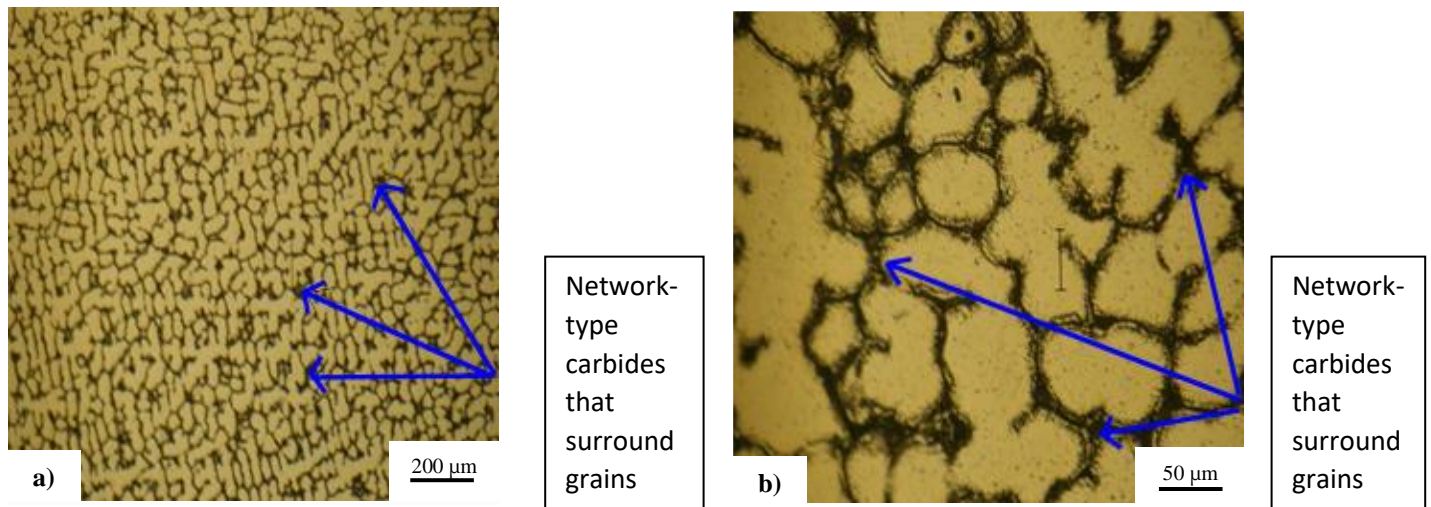


**Figure 2.** As-Cast Microstructure of The Austenitic Steel Obtained By Optical Light Microscope In Two Different Magnifications

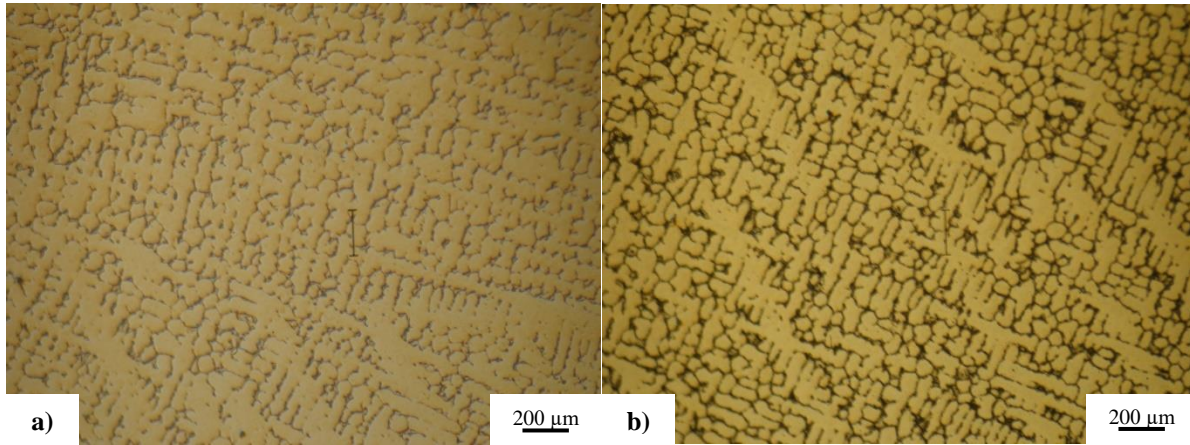


**Figure 3.** Microstructural Images of The Steel Solution Annealed **a)** at 1150 °C for 24 Hours **b)** at 1200 °C for 24 Hours

Eutectic carbides were partially dissolved in austenitic matrix and residual carbides evolved to spherical morphology during 24 hours of solution annealing performed at 1250 °C as seen in the micrograph given in Figure 4-a. Amount of  $M_2C$  carbides was decreased by 48 hours of solution annealing performed at the same temperature as seen in the micrograph given in Figure 4-c. When the duration of solution annealing performed at the same temperature was increased to 72 hours, as seen in the micrograph given in Figure 4-e,  $M_2C$  carbides were fully dissolved.

Average austenite grain size was measured as 50  $\mu\text{m}$  for as-cast austenitic steel and this value increased to 60  $\mu\text{m}$  after solution annealing heat treatment performed at 1250 °C for 24 hours. When soaking time was increased grain coarsening occurred; i.e. average austenite grain size was measured as 120  $\mu\text{m}$  after 48 hours of soaking. All carbides were dissolved and a complete austenite phase was provided by 72 hours of soaking performed at 1250 °C after which average austenite grain size was measured as 160  $\mu\text{m}$  (Figure 4-f).

### 3.1.2 Scanning electron microscopy examination

Scanning Electron Microscope (SEM) micrographs that focus on the eutectic carbides which were present in the as-cast steel (Figure 5-a) and the spherical carbides which were formed as a result of the solution annealing treatment (Figure 5-b) are given in Figure 5 together with the micrographs that indicate  $M_2C - M_6C$  transformation which occurred during the aging treatments performed in two different conditions (Figures 5-c, 5-d, 5-e and 5-f). EDS analysis values detected in the selected and numbered regions related to the both carbides are given in Table 2.

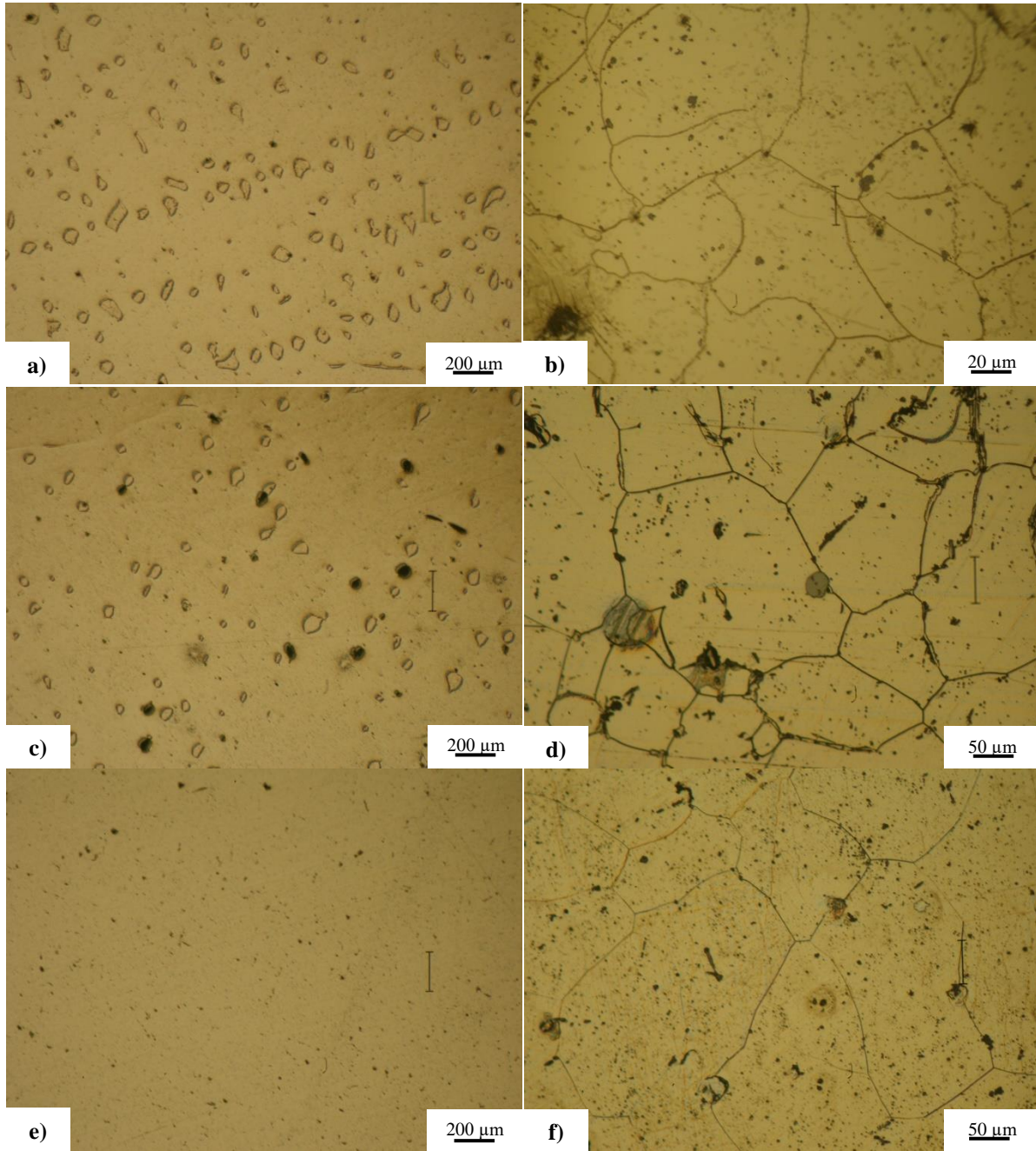


**Figure 4.** Microstructural Images Of The Steel Solution Annealed **a-b)** at 1250 °C for 24 Hours, **c-d)** at 1250 °C for 48 Hours and **e-f)** at 1250 °C for 72 Hours

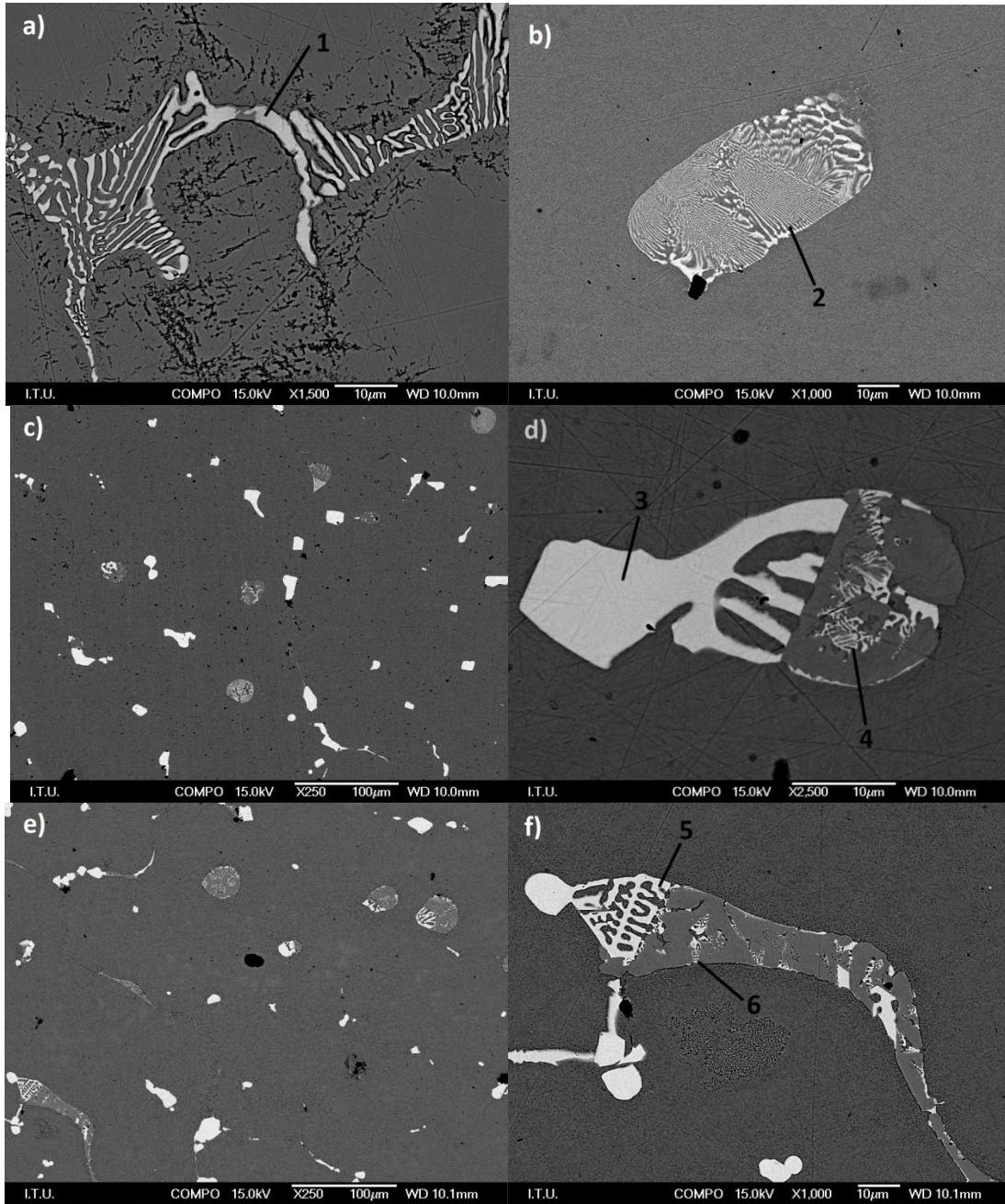


**Figure 5.** a) SEM Micrograph of Eutectic  $M_2C$  Carbide in As-Cast Austenitic Steel b) Spherical  $M_2C$  carbide In the Steel Solution Annealed at 1250 °C for 24 hours c – d)  $M_2C \rightarrow M_6C$  Transformation After Aging at 700 °C for 24 hours e – f)  $M_2C \rightarrow M_6C$  Transformation After Aging at 800 °C for 9 Hours

**Table 2.** EDS Analysis of The Carbides in wt. %

Analysis	Carbide Type	C	Cr	Mn	Fe	Mo
1	$M_2C$	16.60	11.50	0.44	8.97	62.49
2	$M_2C$	21.43	11.27	2.53	11.30	53.47
3	$M_6C$	9.48	4.77	1.23	30.48	54.04
4	$M_2C$	17.76	11.51	0.95	11.17	58.61
5	$M_6C$	9.67	5.04	1.02	30.22	54.05
6	$M_2C$	18.70	11.70	1.85	10.95	56.80

$M_2C$  eutectic carbides were dissolved in austenitic matrix during solution annealing performed at 1250 °C for 24 hours. Residual carbides, starting to transform into  $M_6C$  carbides, evolved to spherical morphology because of aging performed at 700 °C and 800 °C,

as seen in the images given in Figure 5-d and 5-f. Presence of the both carbides within an individual precipitate because of an incomplete transformation can be observed in these two images.

### 3.1.3. Transmission electron microscopy investigation

Transmission Electron Microscopy micrographs of the sample that was solution annealed at 1235 °C for 10 hours and aged at 800 °C for 6 hours are given in this subsection. Selected Area Electron Diffraction Pattern (SAEDP), Bright Field (BF) image and Dark Field (DF) image of the precipitates, Cr<sub>7</sub>BC<sub>4</sub>, Cr<sub>23</sub>C<sub>6</sub> and Mo<sub>2</sub>B are presented.

SAEDP, BF image and DF image of Cr<sub>7</sub>BC<sub>4</sub> precipitate within the sample that was solution annealed at 1235 °C for 10 hours and aged at 800 °C for 6 hours are given in Figures 6-a, 6-b and 6-c respectively. The shiny region that caused the diffraction in the Dark Field image is the part where Cr<sub>7</sub>BC<sub>4</sub> structure was present.

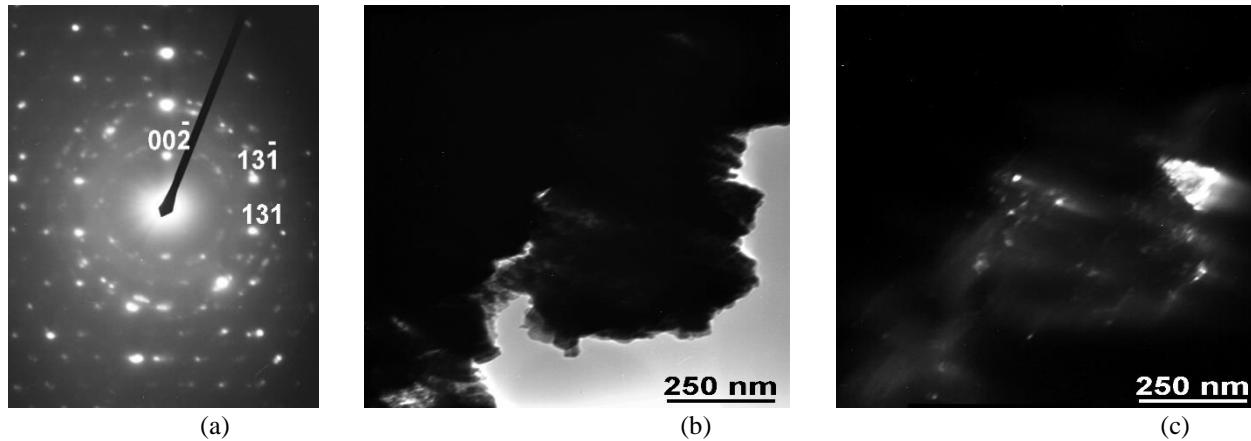


**Figure 6.** a) Selected Area Electron Diffraction Pattern (SAEDP), b) Bright Field (BF) IMAGE and c) Dark Field (DF) Image of Cr<sub>7</sub>BC<sub>4</sub> Precipitate Within The Sample That Was Solution Annealed at 1235 °C for 10 Hours and Aged at 800 °C for 6 hours

SAEDP, BF image and DF image of Cr<sub>23</sub>C<sub>6</sub> precipitate within the sample that was solution annealed at 1235 °C for 10 hours and aged at 800 °C for 6 hours are given in Figures 7-a, 7-b and 7-c respectively. The shiny region in the Dark Field image is the part where Cr<sub>23</sub>C<sub>6</sub> structure was present and that caused the diffraction.

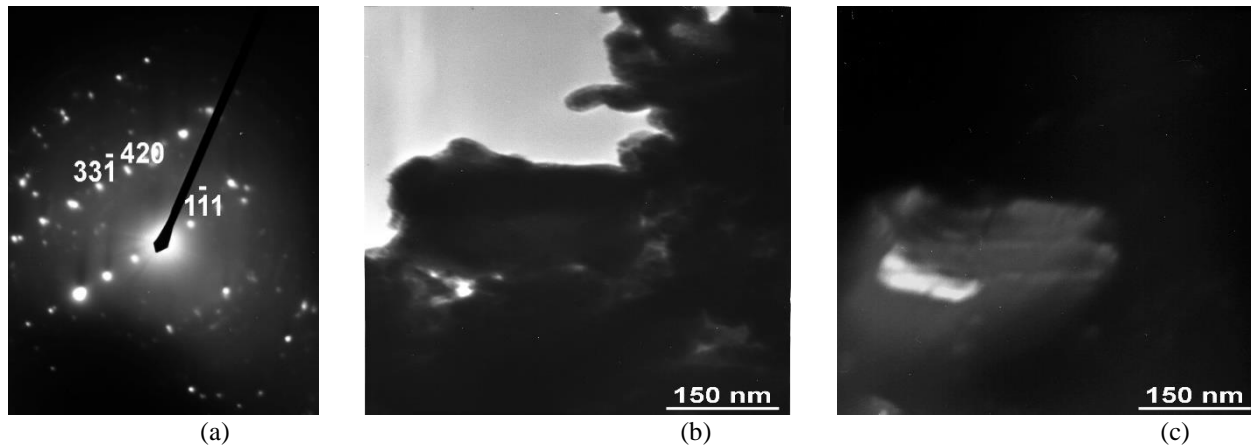


**Figure 7.** a) Selected Area Electron Diffraction Pattern (SAEDP), b) Bright Field (BF) Image and c) Dark Field (DF) Image of Cr<sub>23</sub>C<sub>6</sub> Precipitate Within The Sample That Was Solution Annealed at 1235 °C for 10 Hours and Aged at 800 °C for 6 Hours

SAEDP, BF image and DF image of Mo<sub>2</sub>B precipitate within the sample that was solution annealed at 1235 °C for 10 hours and aged at 800 °C for 6 hours are given in Figures 8-a, 8-b and 8-c respectively. The shiny region in the Dark Field image is the part where Mo<sub>2</sub>B structure was present and that caused the diffraction.

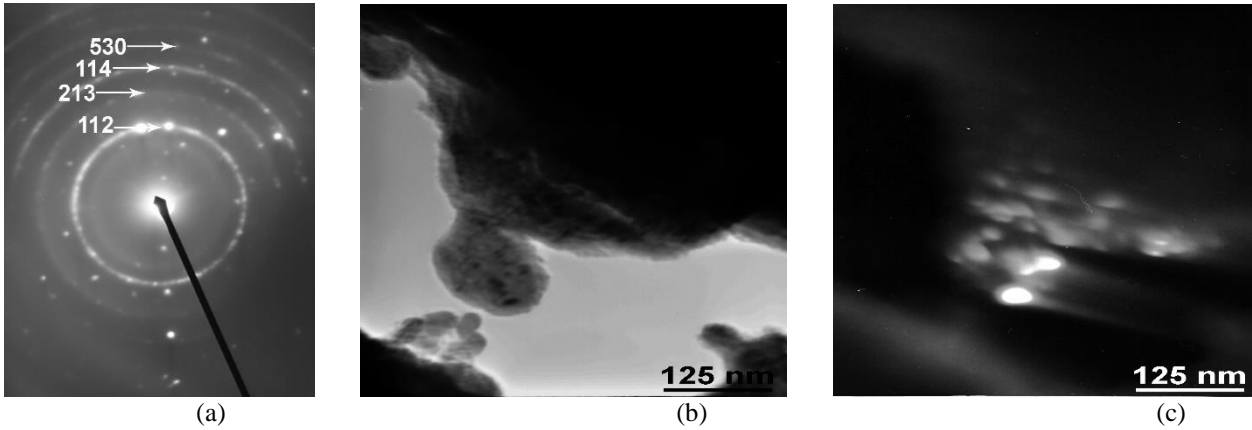


**Figure 8.** a) Selected Area Electron Diffraction Pattern (SAEDP), b) Bright Field (BF) Image and c) Dark Field (DF) Image of Mo<sub>2</sub>B Precipitate Within The Sample That Was Solution Annealed at 1235 °C for 10 Hours and Aged at 800 °C for 6 Hours

In TEM investigations, precipitates of Cr<sub>7</sub>BC<sub>4</sub>, Cr<sub>23</sub>C<sub>6</sub> and Mo<sub>2</sub>BC were detected besides the eutectic carbide structures. Aging treatment that was performed at 800 °C caused the occurrence of submicron-sized Mo<sub>2</sub>B precipitates. It is thought that Cr<sub>23</sub>C<sub>6</sub> structure was nucleated and transformed during the aging period from Cr<sub>7</sub>C<sub>3</sub> structure which was formed during the solution annealing period.

### 3.2. Hardness

Measured hardness values of the cast austenitic steel which was solution annealed at 1250 °C for 24 hours and aged at 550, 600, 700 or 800 °C for different soaking times are given in Table 3 together with standard deviation values. The hardness value of the as-cast austenitic steel was measured as 347±3.5 HV<sub>30</sub> that did not significantly change after solution annealing performed at 1150 °C for 24 hours (344±2.6 HV<sub>30</sub>) and at 1200 °C for 24 hours (339±3.1 HV<sub>30</sub>). However, hardness value was decreased to 286±2.0 HV<sub>30</sub> due to dissolution of some M<sub>2</sub>C carbides in austenite phase and evolution to spherical morphology both of which were caused by solution annealing performed at 1250 °C for 24 hours. Hardness value was measured as 261±3.5 HV<sub>30</sub> after solution annealing performed at 1250 °C for 48 hours and it was further decreased to 223±4.0 HV<sub>30</sub> after solution annealing performed at the same temperature for 72 hours due to dissolution of all carbides and grain coarsening mentioned in Section 3.1.1.

**Table 3.** Measured Hardness Values Of The Cast Austenitic Steel; Solution Annealed at 1250 °C for 24 Hours and Then Aged at 550, 600, 700 or 800 °C for Different Durations Together With Standard Deviation Values

Aging temperature, °C	Duration, hour						
	1	2	3	6	9	12	24
	Hardness value, HV <sub>30</sub>						
550	268±3.0	270±1.5	266±2.0	271±2.1	267±2.6	270±3.5	270±2.6
600	269±2.6	272±2.1	269±3.1	270±2.6	265±2.6	269±3.0	271±3.1
700	293±2.6	319±4.0	367±3.0	402±5.6	432±4.6	511±8.0	686±10.1
800	528±7.0	661±7.5	669±9.5	687±8.2	706±9.2	678±13.1	586±9.5

## 4. Discussion

This section offers more detailed comments on these results and contains explanations collected from the literature.

When the chemical composition value of the steel is integrated into Equation 1, M<sub>s</sub> temperature is calculated as -127 °C, which means that even if rapid cooling is applied from a high temperature down to room temperature, the austenite phase will remain stable and no martensite will be formed within the steel. This finding proves that the steel sample used in this study had an austenitic matrix.

In steels, according to Balluffi and Mehl (1982), increase of elemental boron amount at grain boundaries is achieved by three mechanisms; which are equilibrium segregation, non-equilibrium segregation and extensive segregation. Banerji and Morral (1980) stated that equilibrium segregation occurs as a result of intensive diffusion of solution atoms at high temperatures while the free interfacial energy is decreased because of the diffusion. The segregated atoms are located at grain boundaries in the form of an atomic layer. Non-equilibrium segregation is a dynamic process that occurs during cooling and causes generation of large regions which have been enriched in the solute. This enrichment is a result of the diffusion of vacancy/boron atom pair towards the grain boundary. If diffusion extends along grain boundaries and/or dendrites during solidification of the segregated elements, this phenomenon can be defined as extensive segregation (Jin et al., 2015).

Dendritic microstructure is formed during solidification of cast steels. Chau et al. (2006) claimed that since the austenitic steel sample contained carbide-forming elements such as molybdenum and chromium, network eutectic  $M_2C$  carbides were formed in inter-dendritic spaces due to the segregation of carbon and carbide-forming elements. It was stated by Zhou et al. (2012) that  $M_2C$  carbides are generated by the eutectic reaction,  $L \rightarrow M_2C + \text{austenite}$ , the process of which is accompanied by the element diffusion in the liquid steel. These eutectic carbides can then be broken down into smaller carbides as a result of hot deformation (e.g., forging) or mechanical fragmentation. According to Godec et al. (2015), another possibility is to anneal the steel so that the exchange of elements is driven by diffusion processes. During annealing, the primary and eutectic carbides are dissolved in matrix.

The solubility of boron in  $\gamma$ -iron, austenite, ranges between 0.0055 and 0.2600 wt. % above 925 °C. The boron content in the steel sample used in this study is 0.0093 wt. %, which lies within this solubility range. Bialobrzeska (2021) reported that a hardenability increase can be provided by a boron addition of only 5 ppm (0.0005 wt. %) if a low-alloyed Cr steel is the case. In an experimental study performed by Asahi (2002), it was claimed that boron content which is ideal for hardenability, i.e. the optimum boron content, is increased with increasing molybdenum content and that a molybdenum content of about 0.5 wt. % increases the optimum boron content by more than 100%. It is not surprising for the molybdenum content of almost 5 wt. % in the steel sample used in the current study to influence this optimum boron content significantly. Asahi (2002) also pointed out the formation of coarse borocarbides like  $M_{23}(B,C)_6$  due to non-equilibrium segregation if the boron content exceeds the solubility limit.

M in  $M_2C$  carbides refers to molybdenum, chromium, manganese or iron, which take part in EDS analysis results given in Table 2. Especially chromium and manganese that are dissolved in  $M_2C$  make the carbides more stable for high-temperature applications (Mendez et al., 2004). Solution annealing treatments performed at 1150 and 1200 °C were not able to facilitate the dissolution of  $M_2C$  carbides in austenite phase, as seen in the micrographs given in Figure 3-a and 3-b. Since  $M_2C$  carbides were not dissolved, hardness value of the as-cast steel sample and values of the steel samples solution annealed at 1150 and 1200 °C for 24 hours are very close.

Eutectic  $M_2C$  carbides started to be dissolved at 1250 °C as seen in the micrographs given in Figure 4-a and then residual  $M_2C$  carbides evolved to spherical morphology leading to a decrease in their surface energy and the achievement of a more stable state (Bin et al., 2011). Due to the prolonged soaking performed at 1250 °C, more  $M_2C$  carbides were dissolved in austenite phase which was completely provided during the period of 72 hours. Grain boundary pinning mechanism occurred by the presence of stable  $M_2C$  carbides at elevated temperatures while grain coarsening started at 1250 °C during 24 hours of soaking due to the dissolution of carbides in matrix, finally, average austenite grain size reached 150  $\mu\text{m}$  after the dissolution of all carbides. Following aging treatments were applied only after the solution annealing treatment that was performed at 1250 °C for 24 hours since further annealing would result in excessive enlargement of the grains and lead to unrequired economical and timely consumption.

Padilha and Rios (2002) reported that the diffusion of alloying elements in austenite can be very slow and thus, aging time required to form precipitates in austenite matrix is much longer than that in martensite matrix. In this study, different aging temperatures such as 550, 600, 700 and 800 °C were chosen and almost no hardness increase was observed after aging treatments performed at 550 and 600 °C for 24 hours because of low diffusion rate of the alloying elements in austenite phase at these comparably low temperatures.

Two simultaneous metallurgical mechanisms were observed during the aging treatment performed at 700 and 800 °C. One of these mechanisms is the transformation of  $M_2C$  carbide with a hexagonal lattice into Fe-rich  $M_6C$  carbide with a face-centered cubic lattice. SEM micrographs indicating  $M_2C \rightarrow M_6C$  transformations are given in Figure 5-c, 5-d, 5-e and 5-f and EDS analysis values of both carbides are given in Table 2. In the micrographs given in Figure 5-d and 5-f, it is understood that  $M_2C \rightarrow M_6C$  transformation had not been completed and both of the phases were present within the related precipitates. The  $M_2C$ /matrix interface is a preferential location for the start of  $M_2C$  decomposition. Presumably, molybdenum diffuses from the center of  $M_2C$  to the interface while iron undergoes reverse diffusion. In the decomposed product of  $M_6C$ , in particular, iron content is high. This indicates that  $M_2C$  takes in iron from matrix and is precipitated into  $M_6C$ , as stated by Chen et al. (2016). The other mechanism observed during the aging treatments is the formation of precipitates.

A particular Gibbs energy is required as a driving force for the occurrence of physical phenomena, such as nucleation and subsequent growth of a new phase. This driving force is consumed as economically as possible during the physical phenomenon by minimizing the energies required to form new interfaces, i.e. surface free energy and volume free energy, and for the necessary elastic strain. This effect is achieved by an optimum lattice fit between the matrix and the growing particle. This fit is characterized by a lattice correlation between matrix and new phases which is described by a particular orientation relationship of the two crystal lattices. The particle gains an optimum shape with extended coherent interfaces if the sum of interface energies and strain energy is minimized. Cubes, prisms, plates or needles are formed depending on the particular physicochemical condition. With increasing particle size, the elastic energy, which is proportional to the particle volume, is increased faster than the energy of the initially coherent interface. This effect causes the formation of misfit dislocations in the interface which on one hand increase the interface energy, thus the particle becomes only partially coherent. On the other hand, the misfit dislocations relax coherency stresses leading the resulting energy reduction into being larger than the interface energy increase. With increasing coherency loss, the energies of different interface configurations differ less

and this situation may induce the particle to change its shape and, in particular, to become more spherical (Pitsch and Sauthoff, 1992), as seen related to the carbides investigated in this study.

The diffusion-controlled growth rate is the upper limit for the kinetics of precipitates. However, the diffusion-controlled growth rate decreases with increasing precipitate size, whereas the reaction-controlled growth does not depend on precipitate size. Thus, even if the interface reaction controls growth initially, there will be a transition into diffusion-controlled growth at a critical precipitate size depending on the temperature. Another reason for inhibited growth occurrence may be the presence of usually neglected elastic stresses which are caused by volume differences and misfits between matrix and the precipitate. Even for precipitates without misfit problems, the diffusion fluxes of the various alloying elements give rise to volume differences with related elastic stresses if the respective motions are different (Pitsch and Sauthoff, 1992).

In this study, submicron-sized precipitates formed in the matrix, which were  $\text{Cr}_{23}\text{C}_6$  and  $\text{Mo}_2\text{BC}$  obtained after aging at 700 °C and  $\text{Cr}_{23}\text{C}_6$ ,  $\text{Mo}_2\text{B}$  and  $\text{Cr}_7\text{BC}_4$  obtained after aging at 800 °C, were the sources of hardness increase. Hardness started to decrease after 9 hours of aging which was carried out at 800 °C. This phenomenon possibly resulted from the occurrence of the precipitate coarsening and dissolving in matrix during aging performed at 800 °C for longer times. The situation of different precipitates having grain sizes different from each other, i.e.  $\text{Cr}_{23}\text{C}_6$  precipitates being coarser than  $\text{Mo}_2\text{BC}$  precipitates, may be caused by different diffusion coefficients possessed by different elements.

Hardness comparison of the cast austenitic steel aged at 550, 600, 700 and 800 °C for different durations is outlined in a chart in Figure 9. According to the chart, it is clearly seen that the aging treatments performed at 550 and 600 °C did not lead to any hardness increase. Even though hardness increased gradually at 700 °C, it increased rapidly at 800 °C. It was already reported by Llewellyn and Hudd (1998) that a higher aging temperature provides a higher diffusion rate of a metal leading to an earlier nucleation of precipitation that causes a rapid increase in hardness. Hardness value of the steel that was solution annealed at 1250 °C for 24 hours was  $286 \pm 2.0 \text{ HV}_{30}$ , whereas it was increased by almost 100% during 1 hour of aging at 800 °C and almost 150% after 2 hours of aging at the same temperature. The observed hardness increase was relatively low when aging was carried out for longer than 2 hours at the same temperature. It is pointed out in the chart that the hardness value was  $661 \pm 7.5 \text{ HV}_{30}$  after 2 hours of aging and that it was further increased to a relatively low value of  $706 \pm 9.2 \text{ HV}_{30}$  at the end of 9 hours of aging.

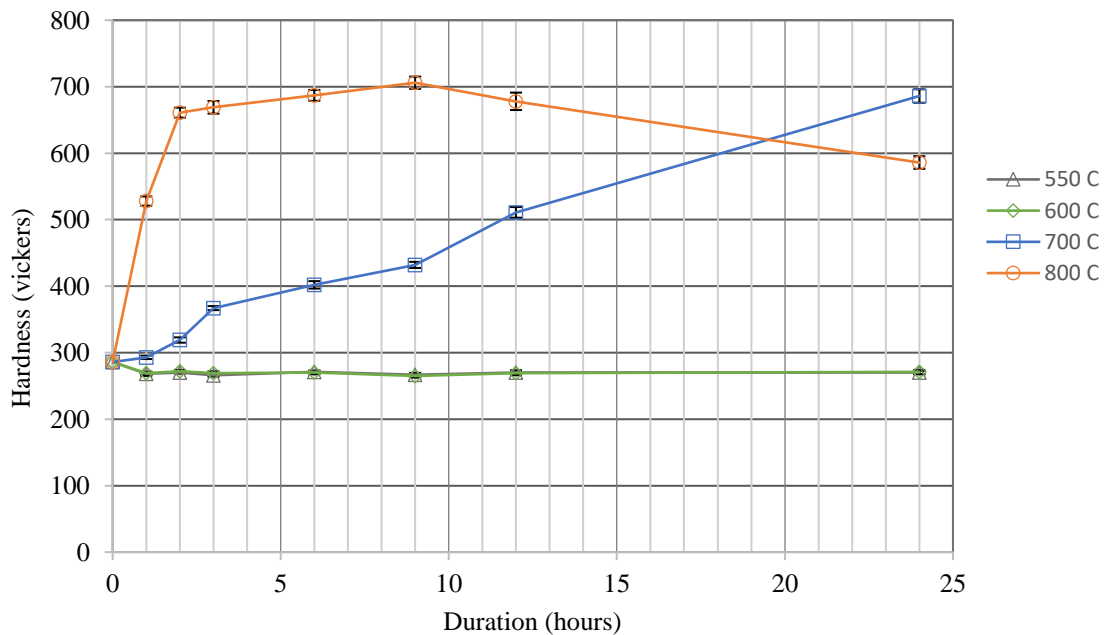


**Figure 9.** Hardness change with soaking time at four different aging temperatures, 550, 600, 700 and 800 °C

## 5. Conclusion

To investigate the effects of the chemical composition and the heat treatment periods on the microstructure and metallurgical properties, a special kind of boron-added cast austenitic steel, about which no study had been performed in the literature before, was cast and heat treated. It was aimed to search for the optimum heat treatment procedure for the dissolution of carbides that cause brittleness and the precipitation of carbide and boride phases that provide hardness to steel. Influence of the generated phases on hardness was observed in the aspect of the applied heat treatment procedures. The phase analyses were performed by energy-dispersive X-ray spectroscopy

and transmission electron microscopy. The current study related to manufacturing, chemical composition and heat treatment processes of this special kind of boron-added cast austenitic steel revealed the following conclusions:

Network-type eutectic  $M_2C$  carbides, which make the steel brittle, were formed during the solidification of the steel. Besides  $M_2C$  carbides, submicron-sized  $Cr_3C_2$  and  $Mn_{23}C_6$  structures were detected within the as-cast sample. Hardness value of the as-cast sample was HV 347 and the average grain size of this sample was approximately 50  $\mu m$ .

To dissolve these  $M_2C$  carbides which are present in the as-cast structure of the steel, solution annealing heat treatments were performed. Since the maximum solubility of boron in iron occurs at 1170 °C, temperatures for the application of solution annealing treatments were chosen close to this value as 1150 and 1200 °C. However, solution annealing treatments performed at 1150 and 1200 °C for 24 hours did not lead to the dissolution of these stable carbides in austenitic matrix. Nevertheless, another solution annealing treatment carried out at a higher temperature of 1250 °C for the same duration caused the structure of a significant amount of these network-type eutectic carbides to transform into a spherical morphology, being dissolved in austenitic matrix, providing a decrease in their surface energies to achieve a thermodynamically more stable state. Dissolution of the carbides and evolution of these carbides to spherical morphology led to a decrease in hardness, down to HV 286, although the grain coarsening occurred only at a negligible level, causing an increase in the grain size up to an average value of 60  $\mu m$ . Amount of  $M_2C$  carbides was decreased further by 48 hours of solution annealing performed at the same temperature and finally,  $M_2C$  carbides were fully dissolved by solution annealing at 1250 °C for 72 hours. Furthermore, the grain growth mechanism started to become active after 24 hours of annealing resulting in an increase in average grain size from 60 to 160  $\mu m$  by the end of solution annealing carried out for 72 hours.

Aging treatments were carried out at four different temperatures after solution annealing performed at 1250 °C for 24 hours. Neither precipitates nor hardness increase were observed after aging performed at 550 and 600 °C for 24 hours. However, precipitates caused an increase in the hardness value by 156% during aging performed at 700 °C for 24 hours. The hardness value of HV 293 measured after one hour of aging was increased up to HV 686 at the end of the 24-hour period. Nucleation of precipitates such as  $Cr_{23}C_6$ ,  $Cr_7BC_4$ ,  $Mo_2B$  and  $Mo_2BC$  in the matrix led to this hardness increase. On the other hand, hardness value which was increased until the end of 9 hours started to decline after this duration when aging treatment was performed at 800 °C, from HV 706 down to HV 586. Possible reasons for hardness decrease were the occurrence of the precipitate coarsening, particularly  $Mo_2B$ , and dissolution of the carbides in matrix during aging performed for longer durations at 800 °C. Precipitates increased the hardness value by 163% at the end of aging performed at 800 °C for 9 hours.

$M_2C$  carbides began to transform into Fe-rich  $M_6C$  carbides during aging carried out at 700 and 800 °C and these carbides were identified and characterized by SEM. Incomplete transformations were observed within several individual precipitates in which both  $M_2C$  carbide and  $M_6C$  carbide were present. The abundance of these two carbides was proved by the aid of EDS analyses related to the measurement of the element contents stoichiometrically.

Submicron-sized precipitates of  $Cr_7BC_4$ ,  $Cr_{23}C_6$ ,  $Mo_2BC$  and  $Mo_2B$  were detected as a result of solution annealing performed at 1235 °C for 10 hours followed by aging at 800 °C for 6 hours. These phases were identified by the reflection of the related Selected Area Electron Diffraction Patterns.

#### Compliance with ethical standards

The authors declare that they have no conflict of interest. This manuscript has been originated from the MSc thesis of the first author.

#### References

- Asahi, H. (2002). Effects of Mo addition and austenitizing temperature on hardenability of low alloy B-added steels. *ISIJ International*, 42(10), 1150-1155.
- ASTM (2021). E112-13, Standard test methods for determining average grain size.
- ASTM (2023). E92-23, Standard test methods for Vickers hardness and Knoop hardness of metallic materials.
- Balluffi, R. W. & Mehl, R. F. (1982). Grain boundary diffusion mechanisms in metals. *Metallurgical Transactions A*, 13(12), 2069-2095.
- Banerji, S. K. & Morral, J. E. (1980). Boron in austenitic stainless steels. *Warrendale: The Metallurgical Society of AIME*.
- Bhadeshia, H. K. D. H. & Honeycombe, R. W. K. (2006). Steels: Microstructure and Properties (Third Edition). *Elsevier*.

- Bialobrzaska, B. (2021). Effect of alloying additives and microadditives on hardenability increase caused by action of boron. *Metals*, 11, 589.
- Bin, Z., Yu, S., Jun, C. & Zhen-shan, C. (2011). Breakdown behavior of eutectic carbide in high speed steel during hot compression. *Journal of Iron and Steel Research International*, 18(1), 41-48.
- British Standard (2000). BS EN 10020:2000, Definition and classification grades of steel.
- Chaus, A. S., Chovanec, J. & Legerska, M. (2006). Development of high-speed steels for cast metal-cutting tools. *Solid State Phenomena*, 113, 559-564.
- Chen, L., Pei, J., Li, F., Zhang, Y., Wang, M. & Ma, X. (2016). Decomposition reaction of metastable  $M_2C$  carbide in a multi-component semi-high-speed steel. *Metallurgical and Materials Transactions A*, 47(A), 5662-5669.
- Çarboğa, C. (2010). Düşük karbonlu çeliklere bor ilavesinin mikroyapı ve mekanik özellikler üzerine etkisi, PhD Thesis, Gazi University, Ankara (in Turkish language).
- Düzcükoğlu, H. & Çetintürk, S. (2015). Effect of boron addition on mechanical properties of 60SiCr7 steel. *International Journal of Materials, Mechanics and Manufacturing*, 3(2), 117-120.
- Godec, M., Pirtovsek, T. V., Batic, B. S., McGuinness, P., Burja, J. & Podgornik, B. (2015). Surface and bulk carbide transformations in high-speed steel. *Scientific Reports*, 1(11), DOI: 10.1038/srep16202.
- Han, F., Hwang, B., Suh, D., Wang, Z., Lee, D. & Kim, S. J. (2008). Effect of molybdenum and chromium on hardenability of low-carbon boron-added steels. *Metals and Materials International*, 14(6), 667-672.
- Jin, S., Tao, N., Marthinsen, K. & Li, Y. (2015). Deformation of an Al-7Mg alloy with extensive structural micro-segregations during dynamic plastic deformation. *Materials Science and Engineering A*, 628, 160-167.
- Llewellyn, D. T. & Hudd, R. C. (2004). Steels: Metallurgy and applications (Third Edition). *Butterworth & Heinemann*.
- Mendez, J., Ghoreshy, M., Mackay, W. B. F., Smith, T. J. N. & Smith, R. W. (2004). Weldability of austenitic manganese steel. *Journal of Materials Processing Technology*, 153-154, 596-602.
- Okamoto, H. (2004). Boron-iron. *Journal of Phase Equilibria and Diffusion*, 25(3), 297-298.
- Padilha, A. F. & Rios, P. R. (2002). Decomposition of austenite in austenitic stainless steels. *ISIJ International*, 42(4), 325-337.
- Pitsch, W. & Sauthoff, G. (1992). A6: Kinetics and morphology of steel constituents, in: *Steel – A Handbook for Materials Research and Engineering*, Vol.1: Fundamentals. *Springer-Verlag*.
- Putatunda, K. S., Jianghuai, Y. & Gundlach B. R. (2005). Development of austenitic structural steel. *Materials and Design*, 26, 534-544.
- Sharma, M., Ortlepp, I. & Bleck, W. (2019). Boron in heat-treatable steels: A review. *Steel Research International*, 90, 1900133.
- Suskia, C. A. & Oliveira, C. A. S. (2013). Effects of austenitization temperature on the microstructure of 15BCr30 and PL22 boron steels, *Materials Research*, 16(4), 803-810.
- Totten, G. E. (2007). *Steel heat treatment handbook: Metallurgy and technologies* (Second Edition). *CRC Press*.
- Zhou, X. F., Fang, F., Jiang, J. Q., Zhu, W. L. & Xu, H. X. (2012). Study on decomposition behaviour of  $M_2C$  eutectic carbide in high speed steel. *Materials Science and Technology*, 28(12), 1499-1504.